Published by Avanti Publishers

International Journal of Architectural Engineering Technology

ISSN (online): 2409-9821

Interference Effects on the Square and Circular Cross-Sectional High-Rise Buildings Under Turbulent Flows

Cheng-Wei Chen[1], Yi-Chao Li[2] and Yuan-Lung Lo[3*]

[1]*Department of Civil Engineering, Tamkang University, New Taipei City, Taiwan*

[2]*Taiwan Building Technology Center, National Taiwan University of Science and Technology, Taipei, Taiwan*

[3]*Department of Civil Engineering, National Taipei University of Technology, Taipei, Taiwan*

ARTICLE INFO

Article Type: Research Article

Keywords:
High-rise building
Interference effect
Interference factor
Aerodynamic force
High-frequency force balancer

Timeline:
Received: June 17, 2022
Accepted: August 23, 2022
Published: September 19, 2022

Citation: Chen C-W, Li Y-C, Lo Y-L. Interference Effects on the Square and Circular Cross-Sectional High-Rise Buildings Under Turbulent Flows. Int J Archit Eng Technol. 2022; 9: 18-36.

DOI: https://doi.org/10.15377/2409-9821.2022.09.2

ABSTRACT

Estimating the wind-induced responses of high-rise buildings requires a detailed investigation of wind force characteristics and structural dynamics, especially when an existing neighboring building has an equivalent volume at adjacent locations. The interference effects caused by such an adjacent building may seriously alternate the wind loading characteristics on the target building and further affect its responses to safety or habitability evaluation. This research investigates the interference effects on the wind-induced responses of high-rise buildings under turbulent boundary layer flows based on a series of wind tunnel tests. This study mainly concerns three disturbance factors to the interference effects: the approaching turbulent flows, the interference locations, and two typical section shapes of the concerned high-rise buildings. Results show that the terrain effect, the interference location effect, and the shape effect of both the principal and the interfering buildings significantly change the interference mechanism to the aerodynamic force and the estimated responses. The aerodynamic and the response interference factors defined in this study have shown distinct different patterns, indicating the interfered resonant response plays a vital role in dominating the interference mechanism. Finally, discretized maps with a satisfactory 0.5B × 0.5B grid resolution under statistical assumptions are proposed as examples for future codification works.

*Corresponding Author
Email: yllo@mail.ntut.edu.tw
Tel: (+88) 6227712171

1. Introduction

The interference effect has been one of the essential topics in wind engineering society. From the 1960s to the present, several different methodologies have been adopted to explain the interference mechanisms of wind-induced responses. These methods include manufacturing pivot-based aeroelastic models for vibration measurements, installing rigid models with the high-frequency-force-balancer for force measurements, and conducting numerical simulations of computational fluid dynamics (Saunders and Melbourne [1], Surry and Mallais [2], Bailey and Kwok [3], Blessmann and Riera [4], Kareem [5], Taniike and Inaoka [6], Sakamoto and Haniu [7], Taniike [8, 9], Yahyai *et al.* [10], Zhang *et al.* [11], Zhang *et al.* [12], Sun and Gu [13], Khanduri *et al.* [14, 15], Luo *et al.* [16], Thepmongkorn et al. [17], Tang and Kwok [18], Xie and Gu [19, 20], Huang and Gu [21], Cheng *et al.* [22], Zhao and Lam [23], Lam *et al.* [24], Lam *et al.* [25], Hui *et al.* [26], Hui *et al.* [27, 28], Fang *et al.* [29], Kim *et al.* [30, 31, 32], Mara *et al.* [33], Yu *et al.* [34], Lo *et al.* [35], Lo *et al.* [36], Yu *et al.* [37], and Lo *et al.* [38]), and so on. Although the discussions have covered a wide range of sensitive parameters, it is still challenging to integrate those findings with codifications because of their complex nature. It is common to estimate design wind loads for buildings in a code or a standard via estimating its mean and the fluctuating force components separately. The mean component relates directly to the approaching mean wind profile. The fluctuating component is usually calculated by the direct product of the wind force spectrum and the structure's mechanical function (Davenport Chain, Davenport [39]) or by the estimations of background and resonant components of responses. Following the same concept may help define interference factors to indicate the amplification or reduction level caused by interference effects. Xie and Gu [19] conducted a series of high-frequency-force-balancer tests to regress the interfered mean forces of a square-sectional high-rise building affected by a single or dual adjacent rectangular high-rise building. Interference factors were defined and regressed in polynomial forms. Cheng *et al.* [22] applied artificial neural network techniques to train limited experimental data to determine the interference factors with different aspect ratios or shape appearances of two buildings under turbulent boundary layer flows. Mara *et al.* [33] defined factors for wind load and peak response of a square building interfered by an identical upstream building under three different turbulent flows. Although other works were involved in estimating interfered wind loads, most are not based on schematic experiments or lack sufficient information for codification. Currently, GB 50009-2012 [40] and Recommendations for Loads on Buildings (2015) [41] have added qualitative descriptions when designers need to consider interference effects in their designs. In GB 50009-2012 [40], interfering wind loads in the along-wind and across-wind directions are factorized and illustrated in contour plots, similar to those interfered peak responses provided in Recommendations for Loads on Buildings (2015) [41]. However, GB 50009-2012 [40] further includes the interference effects of dual interfering buildings introduced in Xie and Gu [19].

On the other hand, interference effects are not only concerned with structural safety problems but also the residential discomfort problem. Based on systematic wind tunnel experiments, Yu *et al.* [37] have proposed an enveloped interference factor for the interfered acceleration caused by six different interfering buildings with section sizes in the upstream region. However, most works only focus on the upstream interference effects and miss the interference effects from the downstream area (Lo *et al.* [35, 38]). Moreover, the discomfort evaluation based on acceleration calculation should consider the notice from ISO 10137:2007 [42] that "In more complex situations, a combination of modal responses may be required." The information indicates that the practical judgment of whether the discomfort criteria are fulfilled or not should depend on the combined maximum acceleration.

This research intends to examine interference effects on wind load components and the consequent structural responses, including safety and discomfort problems. Three atmospheric turbulent boundary layer flow exposures are simulated to consider the approaching turbulence effects. More than two hundred interference locations, including upstream and downstream regions, are covered in one simulated terrain to provide a wide range of interference effects. Meanwhile, two typical section shapes, square and circular, of the principal and the interfering buildings are adopted to compare two extreme building shape conditions. Similar interference factors defined by Cheng *et al.* [22] are assumed in this study to simplify parametric discussions. Finally, this research evaluates the 80% quantile of design interference factors as one example for future codification works. Compared to the author's previous works and related publications in references, this study investigates a wider interference location range than most related works and adopts three different terrains for discussions. Most associated works

only focus on the upstream interference locations. This study includes the downstream interference effects, identified as significant in amplifying the buildings' vibration. In addition, this study attempts to investigate the interference effects on buildings in circular cross-sections, while most previous works limit their discussions to buildings in square or rectangular cross-sections.

2. Experimental Setup and Interference Factor Definition

2.1. Experimental Setup

Approaching flows are simulated in an atmospheric boundary layer wind tunnel at Tamkang University in Taiwan with a testing section of 2.2 m in width, 1.8 m in height, and 12.0 m in length, allowing the passive development of ideal turbulent boundary layer flows with a length scale of 1/400. Wooden spires and roughness blocks are adequately equipped to simulate eddies in different sizes and proper vertical wind profiles specified by the power law. Figure **1** shows the experimental setting of the principal and interfering buildings in circular cross-sections inside the wind tunnel. It should be noted that those two acrylic models in Figure **1** have not been covered with skin layers to maintain Reynolds number similarity in wind tunnel tests.

Figure 1: Experimental setting of principal and interfering buildings in circular cross-sections.

This study adopts three incidental flow conditions to understand the turbulence effect on the interfering mechanisms: open country (Terrain C, $\alpha = 0.13$), suburban (Terrain B, $\alpha = 0.24$), and urban (Terrain A, $\alpha = 0.32$) terrain exposures. Figure **2** shows the normalized mean wind speed profiles and the turbulent intensity profiles with respect to the corresponding boundary layer heights. The boundary layer heights for three simulated terrains are identified to be 1.18 m for Terrain C, 1.36 m for Terrain B, and 1.48 m for Terrain A, respectively. In Figure **2**, the height (60 cm) of the testing models in this study is also normalized and plotted for comparison. The Pitot tube is set up at the elevation of the model height, providing the reference velocity pressure for force coefficient normalization.

In the first series of experiments, two square cross-sectional prismatical models play critical roles: the principal and the interfering buildings. Both models are in the same size of 10 cm in width and depth and 60 cm in height, giving the same aspect ratio of six and the same model volume, 6000 cm^3. To adopt the application of the high-force-frequency-balancer (HFFB) tests, both models are made rigid and light enough to avoid the high-frequency noise signals and not disturb the estimation of structural responses based on spectral analysis approaches. The interference locations are the intersectional points of the along-wind and across-wind grid lines shown in Figure **3**. Finer intersectional points are arranged in the principal building's close region, while coarse ones are for the farther area. The interference locations are normalized by the building width B in the range of (x/B, y/B) = (-4 – 12, 0 – 7) to cover enough sensitive interfering areas, including the commonly discussed upstream interference regions and those downstream (or downwind) regions of interest in this study. For one simulated terrain, there are 204 interference locations. Including the isolated principal building case, there are 205 experimental cases for one

terrain. In total, this study has conducted 615 experimental cases for investigation. The mean wind speeds under three flows are tuned to 4.5m/s for the habitability design and 9.2 m/s for the safety design. The Reynolds number is then estimated at around 3.2×10^4 and 6.3×10^4, respectively, fulfilling the requirement in AWES-QAM-1-2019 [43] for a standard square building model.

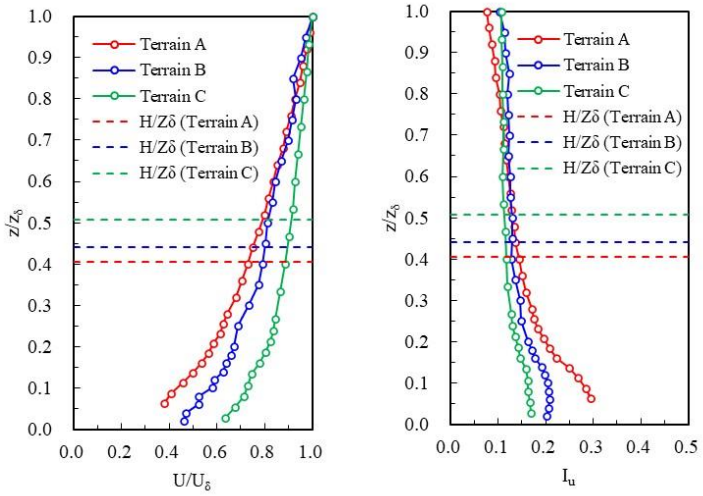

(Terrain A: α = 0.32; Terrain B: α = 0.24; Terrain C: α = 0.13)

Figure 2: Vertical profiles of mean velocity and turbulent intensity.

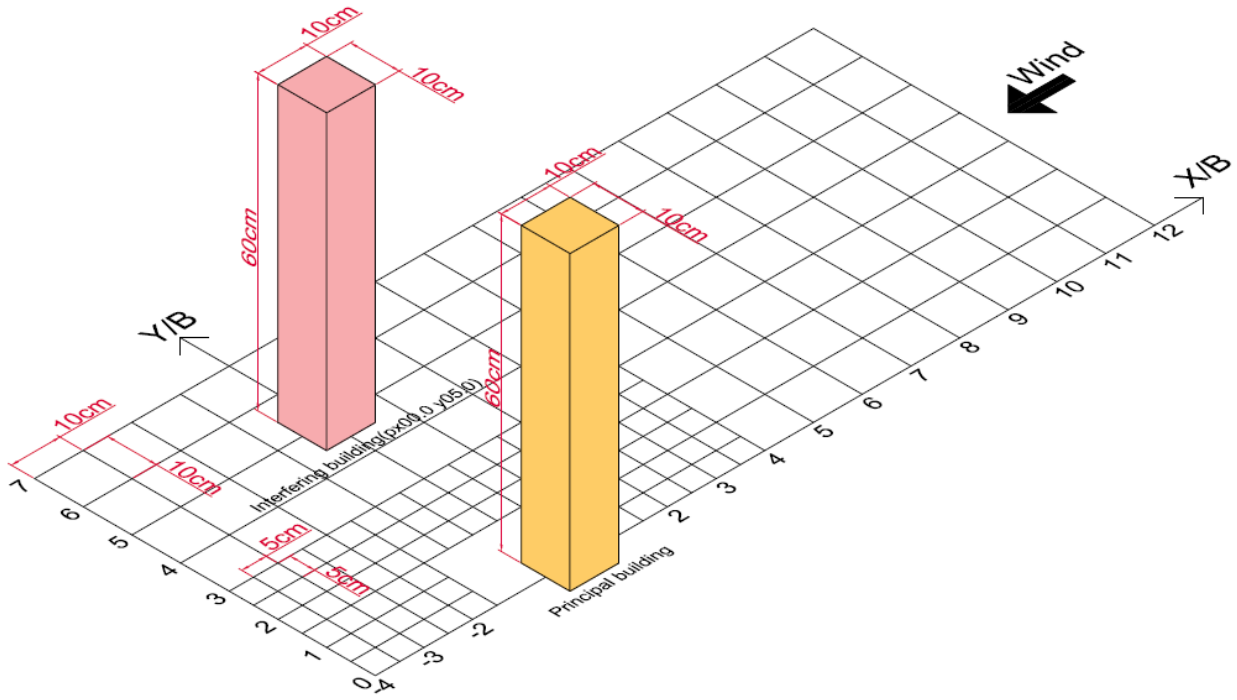

Figure 3: Interference locations in the first experimental phase (all intersectional points).

In the second series of experiments, two square cross-sectional prismatical models are replaced by two circular cross-sectional cylindrical models with the same volume of 6000 cm^3 and an aspect ratio of six. The diameter of the circular section is 11.28 cm, leading to the same area of 100 cm^2 as the square section. Other experimental parameters remain the same for further comparisons, including the same three terrain exposures and interference locations. Unlike the two models in square prismatic shape, the Reynolds number effect should be examined in advance. Usually, the Reynolds number at the field scale should be in the 10^7 - 10^9 range, which is rarely achievable in a conventional wind tunnel simulation. Therefore, this study has covered the model's

appearance with a delicate rough skin layer to increase the Reynolds number. Also, the simulated turbulent flows provide 12-15% turbulence intensity over the model height range. According to Cheng and Fu [44], such turbulence level could help stabilize the flow pattern around the curved geometric model in wind tunnel tests. In this study, the drag coefficient of the isolated circular cross-sectional cylindrical model is 0.65 under the open country terrain flow, as shown in Figure **4**. The drag coefficient variation in black in Figure **4** is given in Holmes and Bekele [45] to illustrate the Reynolds number effects of a circular cylinder in the sub-critical Reynolds number range. The value of 0.65, marked as a star, implies that the Reynolds number is in the subcritical range, not falling in the critical range that underestimates wind forces at the field scale.

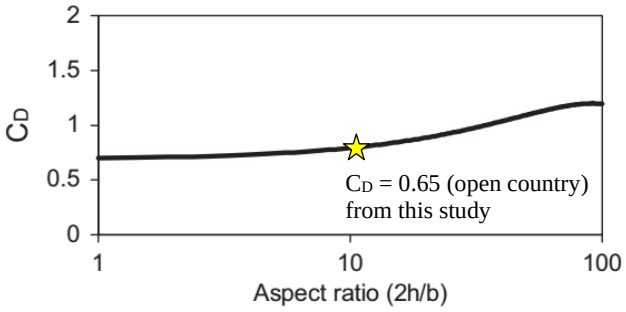

Figure 4: Effect of aspect ratio on the drag coefficient of a circular cylinder in the sub-critical Reynolds number range (Holmes and Bekele [45]).

The JR3 Universal Force-Moment Sensor System from Nitta Co., which can measure three base shears and three base overturning moments of the principal building, is adopted in this study. These six base forces/moments follow the coordinates shown in Figure **5**. The sampling rate is 1,000 Hz and set to record for a continuous 180 seconds for each interference location case. According to Tamura [47, 48], the principal building's fundamental frequency in the field scale is approximately 0.2 Hz for a 240 m high-rise building. Table **1** lists basic information for three simulated terrains and the data sampling conditions. The design wind speeds in Taiwan Wind Code for Buildings 2015 [46] are referenced for the velocity range for the subsequent velocity conversions to cover enough velocity range for discussion. Table **2** lists the concerned design wind speeds at the building heights and the corresponding reduced velocities. Based on Tables **1** and **2**, velocity scale factors and time scale factors are estimated. For example, when reduced velocity equals 7.5, the fundamental frequency is converted to a 12 – 14.8 Hz range for the safety evaluation and a 26 – 32 Hz range for the habitability evaluation. The model's frequency is 82 and 85 Hz via free vibration tests for both building models in square and circular shapes. Although the frequency gap between the actual structure and the model is not ideally far enough, the model's frequency is higher than the structural frequency for the habitability evaluation, which should be acceptably in a good fabrication condition for a model for the HFFB tests.

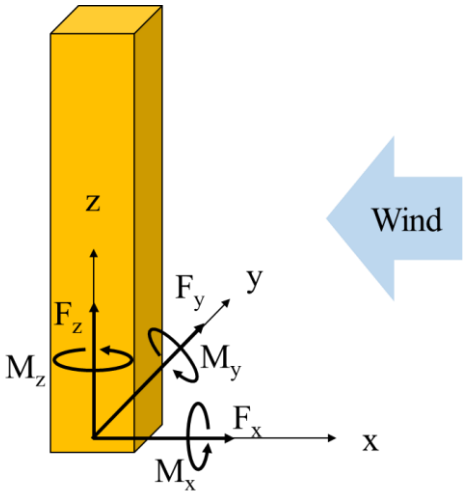

Figure 5: Diagrams of base shears and base overturning moments.

Table 1: Basic information for flow simulations and data sampling

Terrain	A	B	C
Power-law index α	0.32	0.24	0.13
Mean wind speed at the model height U_H(m/s) for a 50-year return period design	9.2	9.2	9.2
Mean wind speed at the model height U_H(m/s) for a 1-year return period design	4.5	4.5	4.5
Sampling rate (Hz)	1000	1000	1000
Sampling length (s)	180	180	180
Length scale (wind tunnel/field) λ_L	1/400	1/400	1/400

Table 2: Design wind speeds at building heights and corresponding reduced velocities

50-year return period for safety design									
Design wind speed at building height U_H(m/s)	66.7	62.5	58.3	54.2	50.0	45.8	41.7	37.5	33.3
Reduced velocity U_r	8.0	7.5	7.0	6.5	6.0	5.5	5.0	4.5	4.0
1-year return period for habitability design									
Design wind speed at building height U_H(m/s)	30.7	28.8	26.8	24.9	23.0	21.1	19.2	17.3	15.3
Reduced velocity U_r	3.9	3.5	3.22	3.0	2.8	2.5	2.3	2.1	1.8

Note: The 1-year-return-period design wind speed is assumed to be 0.46 times the 50-year-return-period design wind speed.

It is worth mentioning that both the windward faces of the buildings are perpendicular to the wind direction. The directional effect from approaching wind is ignored in this study for simplification. In some references, Kim *et al.* [30], the directional effect could be crucial for estimating local peak pressures. However, this is not in this study's concerns.

2.2. Interference Factor Definition

The interference factor is a commonly used scale to indicate how wind loads or structural responses are amplified or reduced by the interference effect. Most references adopted two common experimental terminologies to examine interference effects. The first terminology is the *buffeting factor (BF)*, mainly used to indicate the amplification or reduction in displacement responses, especially for the root-mean-square value of fluctuating displacement at the rooftop. Bailey and Kwok [3] first proposed a buffeting factor to quantify the interference effect identified by the pivot-based aeroelastic tests. The second term is the *interference factor (IF)*, which indicates the amplified or shielded effects on aerodynamic forces. However, the terminology of interference factor has been generally used for both aerodynamic forces and structural responses in recent years. For instance, Mara *et al.* [33] proposed using interference factors to compare peak wind load and response. This study defines interference factors for general discussion, either for aerodynamic forces or structural responses.

In most codes, the high-rise building's design wind load can be described as a combination of the mean component and the fluctuating component of load effects. The approaching flow mainly causes the former component. The latter is due to the incoming turbulence, the flow separation around the building, and the resonance inspired by the structural dynamics. The fluctuating component can be further divided into the background and resonant parts. Cheng *et al.* [22] proposed individual interference factors for load effects of mean component, background component, and resonant component, respectively. For the comparison works of much data in this study, aerodynamic interference factors are defined in Equations (1) and (2) for mean wind force in the along-wind direction and fluctuating wind forces in the along-wind and across-wind directions.

$$IF_{st} = \frac{\bar{F}_{x,intf}}{\bar{F}_{x,iso}} \tag{1}$$

$$IF_i = \frac{\left\{\int_0^\infty S_{F'_{i,intf}}(n)\,dn\right\}^{1/2}}{\left\{\int_0^\infty S_{F'_{i,iso}}(n)\,dn\right\}^{1/2}} \qquad i = x, y \tag{2}$$

where IF_{st} the aerodynamic interference factor of mean wind force in the along-wind direction; $\bar{F}_{x,intf}$ the interfered mean wind force in the along-wind direction; $\bar{F}_{x,iso}$ the mean wind force in the along-wind direction when the principal building is isolated; IF_i the aerodynamic interference factors of fluctuating wind force; $S_{F'_{i,intf}}(n)$ the interfered force spectrum; $S_{F'_{i,iso}}(n)$ the force spectrum without any interference effects. In this study, the torsion is ignored because of the nature of the selected cross-sections.

Equations (3) and (4) are defined to estimate the interference effects on the wind-induced responses. The displacement interference factor, *DIF*, is for discussing the interference effect on the fluctuating displacements at the rooftop, while the acceleration interference factor, *AIF*, is for the fluctuating accelerations.

$$DIF_i = \frac{\sigma_{i,intf}}{\sigma_{i,iso}} = \frac{\sqrt{\frac{1}{k_i^2}\int_0^\infty |H_i(n)|^2 S_{F'_{i,intf}}(n)\,dn}}{\sqrt{\frac{1}{k_i^2}\int_0^\infty |H_i(n)|^2 S_{F'_{i,iso}}(n)\,dn}} \qquad i = x, y \tag{3}$$

$$AIF_i = \frac{\sigma_{\ddot{i},intf}}{\sigma_{\ddot{i},iso}} = \frac{\sqrt{\frac{1}{k_i^2}\int_0^\infty \left(\frac{n}{2\pi}\right)^4 |H_i(n)|^2 S_{F'_{i,intf}}(n)\,dn}}{\sqrt{\frac{1}{k_i^2}\int_0^\infty \left(\frac{n}{2\pi}\right)^4 |H_i(n)|^2 S_{F'_{i,iso}}(n)\,dn}} \qquad i = x, y \tag{4}$$

where σ_i the standard deviation value of fluctuating displacement response; $\sigma_{\ddot{i}}$ the standard deviation value of fluctuating acceleration response; k_i the stiffness values; $|H_i(n)|^2$ the mechanical functions defined in Equation (5), assuming a 1% damping ratio for both along-wind and across-wind directions. The structural frequency $n_{0,i}$ is determined based on the assumptions of 0.2 Hz for a 240 m high-rise building and the time scale factors for the safety and habitability evaluations.

$$|H_i(n)|^2 = \frac{1}{\left[\left(1 - \left(\frac{n}{n_{0,i}}\right)^2\right)^2 + \left(2\xi\left(\frac{n}{n_{0,i}}\right)\right)^2\right]} \qquad i = x, y \tag{5}$$

The above calculations are generally based on the Davenport Chain (Davenport [39]), utilizing the measured overturning moments of the along-wind and the across-wind directions under the assumption of the linear first mode shape. In the following discussions, interference factors are examined in colored contour plots and magnitudes. The contour plots can show the interference effect qualitatively and those sensitive areas. Furthermore, to generalize the results, the idea of the envelope interference factor defined by Yu *et al.* [37] is adopted in this study. The maximum interference factor is selected for discussions among all concerned reduced velocities in Table **2**. Equations (3) and (4) are further generalized as Equations (6) and (7).

$$EDIF_i = max_{all\,V_r}\left(DIF_i(V_r)\right) \qquad i = x, y \tag{6}$$

$$EAIF_i = max_{all\,V_r}\left(AIF_i(V_r)\right) \qquad i = x, y \tag{7}$$

3. Results and Discussions

3.1. Interference Factor for Aerodynamic Force

3.1.1 Mean Component of Aerodynamic Force

Figure **6(a)** shows the colored contour plots to indicate the interference effect tendencies under three terrains. The two-color bar is selected for the contour plots to demonstrate the gradual varying trend concerning the interference locations. The blue color represents a reduction effect; the red color represents an amplification effect. When the color is white, nearly no interference effect is identified. The coordinate system of the interference locations for the contour plots in this paper is based on (x/B, y/B), where x represents the along-wind direction and y represents the across-wind direction. B is the width of the square cross-section.

It is indicated that the interfering buildings located in the upstream regions of the principal buildings strongly reduce the along-wind mean wind force on the principal buildings. The involved upstream area could extend farther than x/B = 10 in the y/B = ±1 lateral range, forming a belt-like region. In Cheng *et al.* [22], this region can reach 14 times the building width. The reduction level is more significant in the square cross-sectional model case than in the circular cross-sectional model case. The terrain effect is more evident in Terrain B and C, showing a more enhanced interference phenomenon than in terrain A. In the two plots of Terrain A, a light red area in the lateral direction of the principal building shows a slight amplification effect, which might be ignorable since the IF value is generally less than 1.2. The most considerable amplification at the location of (x/B = -0.5, y/B = 1.5) in Terrain A shows the IF value is 1.321, which is worth investigating in the future.

In Figure **6(b)**, the contour plots of interference factors for the mean component of along-wind force coefficients in Mara *et al.* [33] are extracted to compare with the corresponding terrains in Figure **6(a)** from this study. Although the contour plots by Mara *et al.* [33] provide a narrower observation range, the tendencies in both plots are pretty consistent with the outcomes of this study, where the upstream interfering buildings generally reduce the mean along-wind force coefficients to locations farther than 12 times building breadth.

3.1.2. Fluctuating Component of Aerodynamic Force

Figure **7** shows the interference effects on the along-wind and across-wind fluctuating wind forces. In Figure **7(a)**, it is interesting to see the distinct differences between Terrain A, B, and Terrain C. No apparent amplification effect is observed in the former two terrains. The belt-like reduction region upstream of the principal buildings is similar to that in Figure **6**. In Terrain C, most of the upstream area of the square principal building shows an amplified fluctuating force; meanwhile, the belt-like reduction region upstream of the principal circular building becomes narrower than that in Figure **6**. The belt width is almost the same size as the diameter of the circular building. Aside from the narrow belt-like reduction area, a wider belt area shows amplification effects. The different area sizes to cause the amplification effects may result from different levels of wake structures behind the two cross-sectional buildings. As a result, the largest amplification (IF_x = 1.339) in the along-wind direction is at the location of (x/B = 2.5, y/B = 1.0) in Terrain C in the square building case. The largest reduction (IF_x = 0.346) is at the location of (x/B = 1.5, y/B = 0.0) in Terrain A in the square building case.

As for the interference effect in the across-wind fluctuating wind forces in Figure **7(b)**, two cross-sectional buildings seem to have the same distribution pattern at a glance. Two different observations can be carefully examined. First, in the square building case, the amplification area increases from Terrain A to Terrain C, indicating the enhanced effect due to the vortex shed from the interfering building. As the incoming turbulence intensity decreases, the vortex structure is less weakened, so the amplification effect in the across-wind direction is more significant. On the other hand, the amplification area in the circular building case remains almost the same size regardless of terrain varying. Second, a reduction effect is generally indicated when the interfering building is located in a close region near the square principal building. The most considerable case is at (x/B = -0.5, y/B = 1.5) showing a large reduction of almost 60%. As a result, the largest amplification in the across-wind direction is IF_y = 1.876 at the location of (x/B = 4.0, y/B = 2.5) in the square building case and IF_y = 1.878 at the location of (x/B = 4.0, y/B = 1.0) in the circular building case, both in Terrain C. The largest reduction is IF_y = 0.436 at the location of (x/B = 1.5, y/B = 0.5) in the square building case in Terrain B. A similar reduction is IF_y = 0.474 at the same location in the square building case in Terrain A.

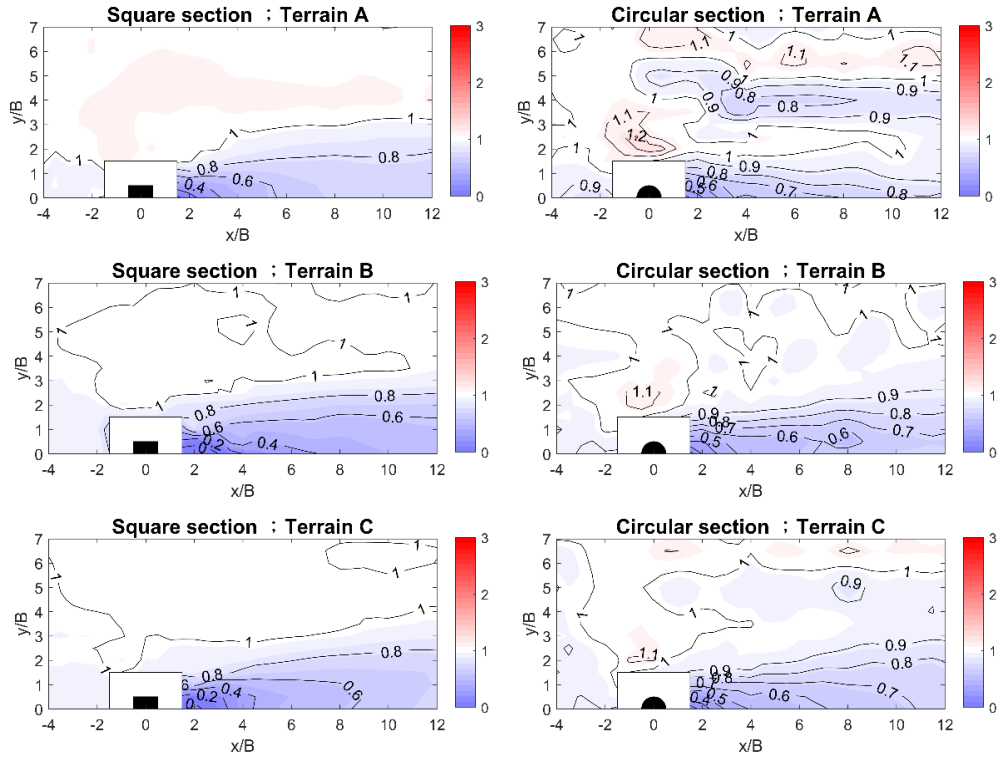

(a) This study

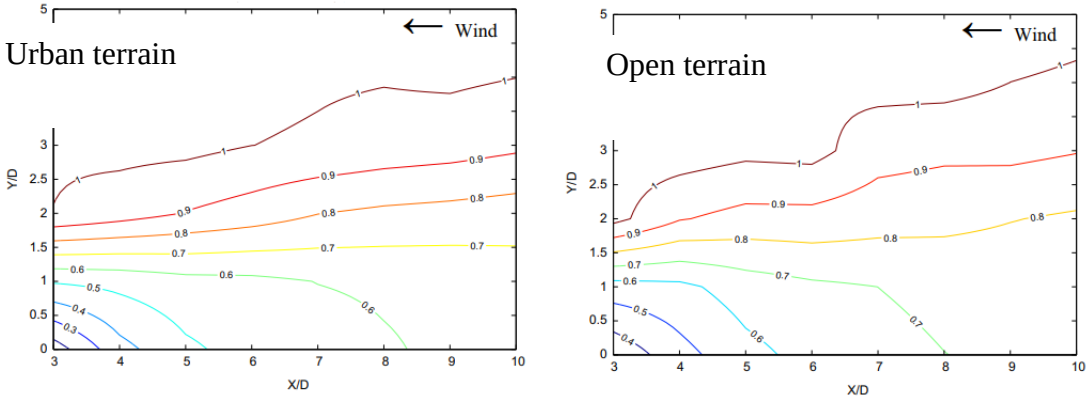

(b) Mara *et al.* [33]

Figure 6: Contours of aerodynamic interference factor IF_{st}.

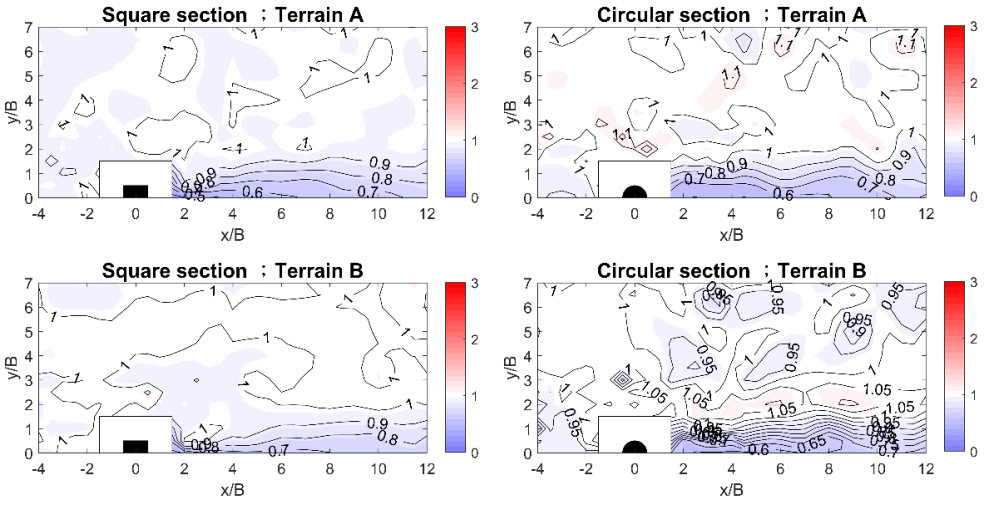

Fig. 7 (contd.....)

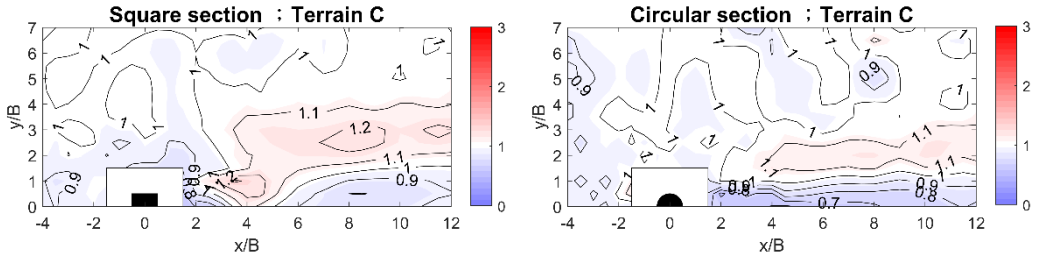

(a) Along-wind IF_x

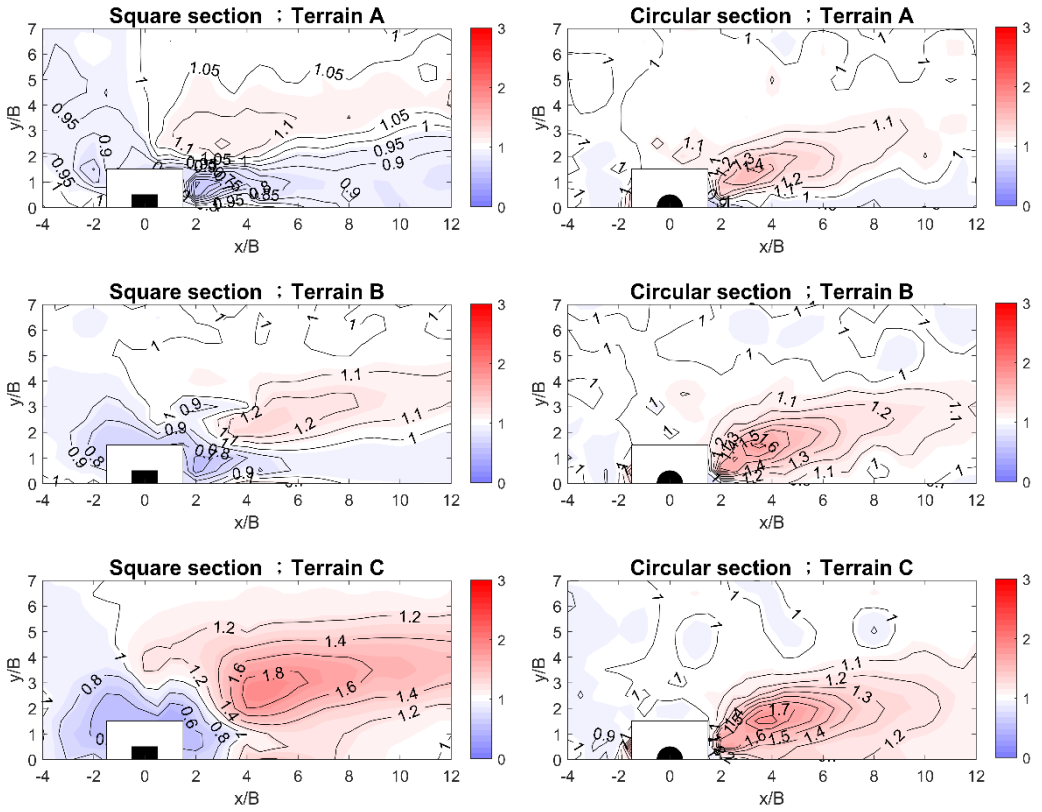

(b) Across-wind F_y

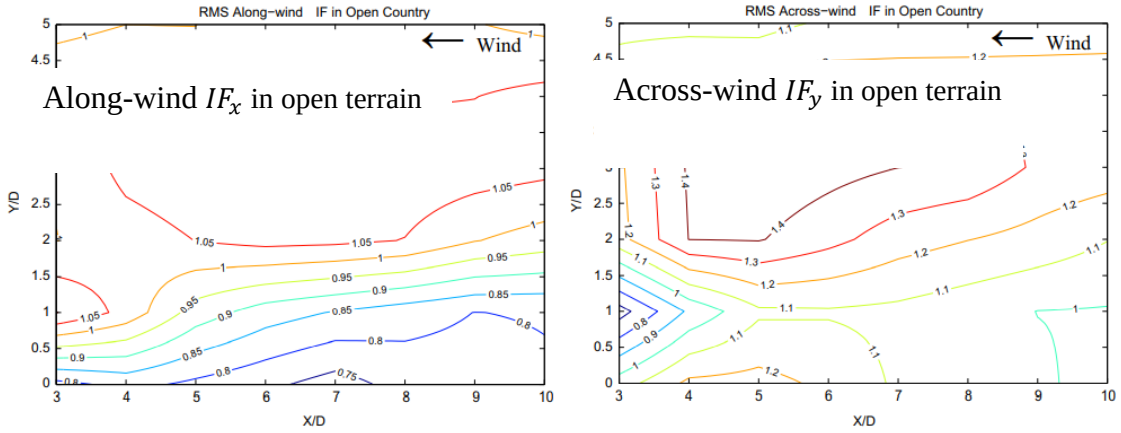

(c) Mara *et al.* [33]

Figure 7: Contours of aerodynamic interference factors: (a) Along-wind IF_x; (b) Across-wind IF_y; (c) Mara *et al.* [33].

Figure **7(c)** shows the contour plots extracted from Mara *et al.* [33] for comparison with the corresponding results in Terrain C in Figures **7(a)** and **7(b)**. Both plots in Figure **7(c)** are part of this study's discussion interference location range. If only focused on the overlapped area, both results show good consistency, as the comparison shown in Figure **6**.

3.2. Interference Factor for Structural Responses

3.2.1. Rooftop Displacement Due to Interference Effects

In the discussion regarding the rooftop displacement, only the fluctuating displacement component is concerned since the mean displacement component can be easily calculated by the static analysis of the interfered mean wind force in the previous section. Although Lo and Kim [49] indicated that the mean force component in the across-wind or the torsional direction could be slightly affected by an existing interfering building, the effect should be small enough to ignore in this study. Figure **8** shows the contour plots of displacement interference factors obtained by Equation (6).

As shown in Figure **8(a)**, the interference-induced amplification in the along-wind fluctuating displacement is strengthened when Terrain A changes to Terrain C for both the square and the circular cases. Unlike Figure **7(a)**, only a limited upstream area in Terrain C shows the amplification effect for the along-wind fluctuating force. Most areas in all terrains in Figure **8(a)** show amplified IF_x values. The discrepancy should be considered as the contribution from the resonant component inspired by the structural dynamics. It is also interesting to indicate that the largest amplification in the along-wind direction is not at the same location for the square and circular building cases. For the square building case, the largest $EDIF_x$ = 1.32 at the location of (x/B = -1.5, y/B = 1.0) in Terrain A gradually increases to 1.49 in Terrain B and further to 2.07 in Terrain C at the same location. This identified location is close to the downstream resonant case of (x/B = -1.5, y/B = 2.2) mentioned in Bailey and Kwok [3]. For the circular building case, the largest $EDIF_x$ = 1.56 at the location of (x/B = 3.0, y/B = 1.5) in Terrain A gradually increases to 2.04 in Terrain B and further to 2.52 in Terrain C at an almost the same location (x/B = 3.0, y/B = 1.0). The amplification condition is larger in the circular building case than in the square building case, which may be due to the smaller fluctuating response of an isolated circular building than an isolated square one. The reduction effect is neglected here based on the conservative design principle compared to an isolated design.

For the across-wind fluctuating displacement in Figure **8(b)**, the amplification and reduction effects are distributed in the square building cases. However, the amplification effect is identified in most interference locations of the circular building cases. In the square building case, the reduction interference effect is indicated in the area upstream of the principal building, and the amplification interference effect is in the area of y/B > 2.0. The areas with amplification and reduction effects are separated with a boundary of y/B = 2.0. Regarding Terrain B, the area size with the reduction effect is shrinkage to the surrounding upstream area near the principal building. When it is Terrain C, the apparent reduction effect is only indicated near the side locations, x/B = -2.0 – 2.0 and y/B = 1.5 – 2.5. The largest reduction effect is found to change from the upstream location of (x/B = 1.5, y/B = 0.5) in Terrain A and B to the side location of (x/B = 1.0, y/B = 1.5) in Terrain C. On the other hand, the amplification effect in the square building case also has a different trend from Terrain A to Terrain C. When it is in Terrain A and B, the amplification effect is in the area where x/B = 4.0 – 10.0 and y/B = 1.5 – 4.0, which is typically indicated in references. However, in Terrain C, besides the typical area, the side/downwind area shows another sensitive interference location to amplify the fluctuating responses. Compared to Figure **7(b)**, the typical area, where x/B = 4.0 – 10.0 and y/B = 1.5 – 4.0, is mutually indicated in interfered fluctuating force and displacement. However, the side/downwind area is only indicated in interfered responses, explaining that the downstream resonant phenomenon near the location of (x/B = -1.5, y/B = 1.0) has a more significant interfered response in the across-wind direction than in the along-wind direction. Nevertheless, the size of such a downwind interference effect seems to have a larger area in the across-wind direction.

In the circular building case, the reduction effect is indicated only in Terrain C, the surrounding area of the principal building. The amplification effect is almost in the same area, no matter the terrain changes. Unlike the square building case, the amplification effect is only found in the typical area of x/B = 2.0 – 10.0 and y/B = 1.0 – 3.0. No side/downwind interference effect is identified, meaning that the downstream resonant phenomenon might

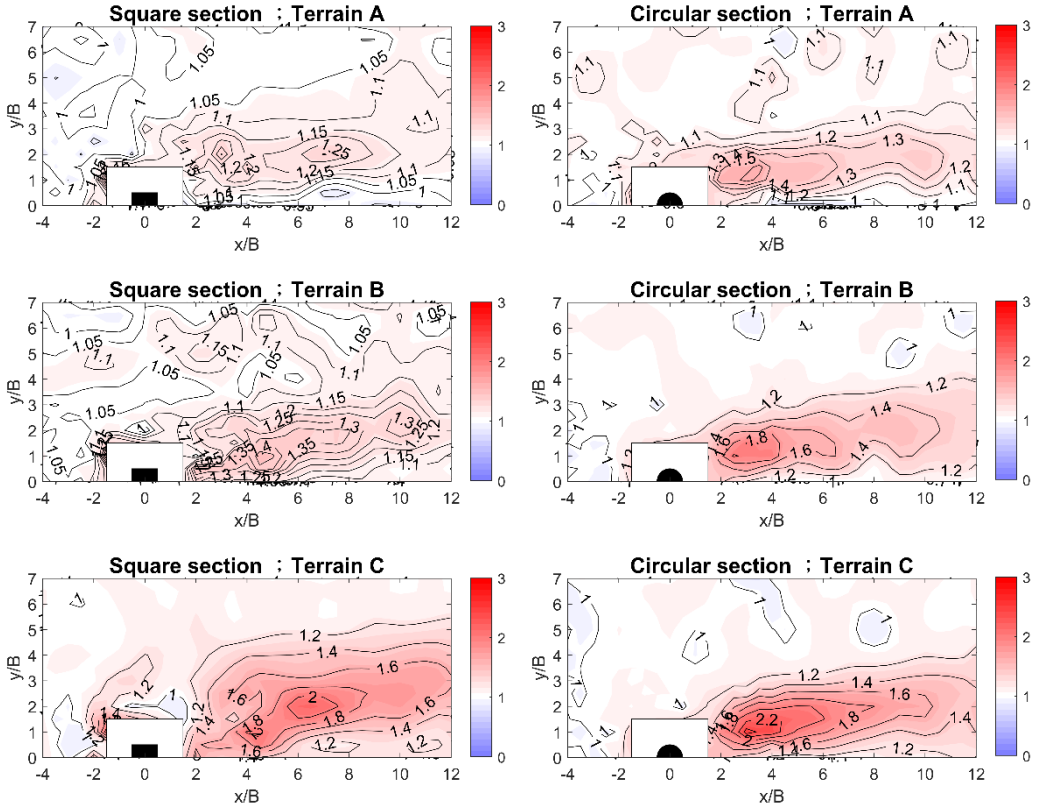

(a) Along-wind $EDIF_x$

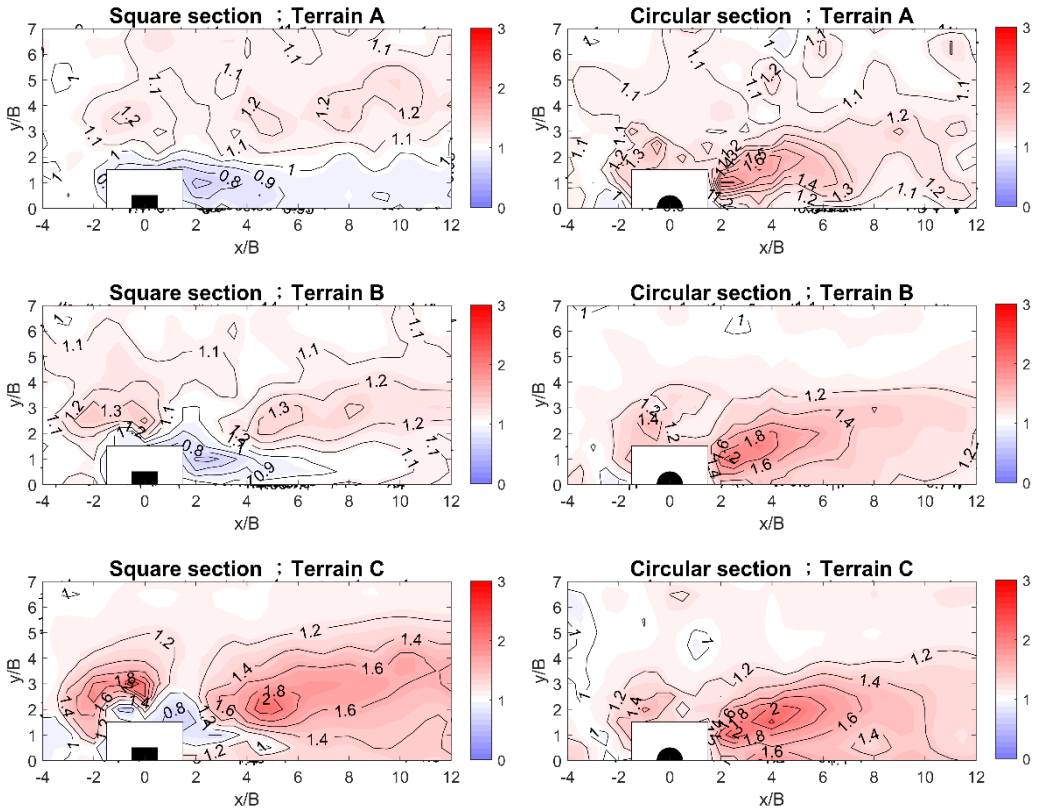

(b) Across-wind $EDIF_y$

Figure 8: Contours of displacement interference factors: (a) Along-wind $EDIF_x$; (b) Across-wind $EDIF_y$.

be only seen for those buildings which can shed a strong vortex/wake to affect the downwind buildings. As a result, no clear reduction effect is in the observed range in the along-wind direction. The largest amplification effect is located at x/B = 3.0 and y/B = 1.0 in the circular building case in Terrain C. In the across-wind direction, the reduction effect is indicated near the principal building, where the most significant reduction effect is at x/B = 1.0 and y/B = 1.5 in the square building case in Terrain C. A similar reduction level is also indicated at almost the same location in the circular building case in Terrain C. The largest amplification effect has different locations in the square and the circular building cases in Terrain C. The former locates at x/B = -0.5 and y/B = 3.0, where the downstream resonant phenomenon is supposed to occur. The latter locates at x/B = 4.0 and y/B = 1.5, where most references indicate the commonly known upstream interference region.

Comparing Figures **7** and **8** shows that although the interference factors for the aerodynamic forces are primarily defined to indicate the amplification or reduction effects, it is more desirable to determine the interference factors for the interfered responses, including the background component and the resonant component, respectively.

3.2.2. Rooftop Acceleration Due to Interference Effects

Figure **9** shows the contour plots of the acceleration interference factors. In the along-wind direction, both the square and the circular building cases have a similar contour pattern as that in Figure **8(a)**. Only the largest amplification effect is a bit closer to the principal building. In the across-wind direction, similar patterns can be seen in both cases compared to that in Figure **8(b)**. However, the significant amplification at the side/downwind location is no longer identified in the square building case, and the circular building case has almost no reduction effect.

3.2.3. Design contours of interfered response estimation

An example of discretized maps of response interference factors is proposed in Figures **10** and **11** for quick reference for an initial design of wind-induced responses due to interference effects. In the discretized maps, a 0.5B×0.5B grid is presumed to be the resolution unit. Several assumptions decide the representative interference factor value in each grid: (1) averaged interference factor is taken from a re-calculation with the damping ratio assumed to be 1% and 1.5%; (2) ensemble size is increased to 50 by elongating the measuring time, and the corresponding interference factor is taken according to the 80% non-exceedance probability position; (3) interference factor is rounded to the first decimal point for reading convenience; (4) interference factor is assumed 1.0 to ignore the reduction effect for the conservative principle of design.

In fact, the acceleration interference factors in the along-wind direction and the across-wind direction can be integrated into one factor if the following Equation (6) is concerned with the corner acceleration.

$$\sigma_A = \sqrt{\sigma_{\ddot{x}c}^2 + \sigma_{\ddot{y}c}^2} \tag{6}$$

where σ_A the equivalent corner acceleration; $\sigma_{\ddot{x}c}^2$ the variance of along-wind acceleration coupled with the twist acceleration effect; $\sigma_{\ddot{y}c}^2$ the variance of across-wind acceleration coupled with the twist acceleration effect. In this study, the twist responses caused by the torsional force are ignored. However, it would be essential to include the torsional effects for those buildings with unsymmetric section shapes or large depth/width ratios for the corner acceleration estimation.

It is well known that the mechanism to cause interference effects involves many disturbance factors. As mentioned before, although some international codes or standards have tried to integrate it with the codifications, a qualitative description could be the only solution to remind the designers to include the modification due to interference effects. The discretized design map in Figures **10** and **11** provides one possible expression of collecting essential data for interference effects. The authors would like to emphasize that the calculated interference factors from different wind tunnel tests should be further integrated with a systematic statistical process.

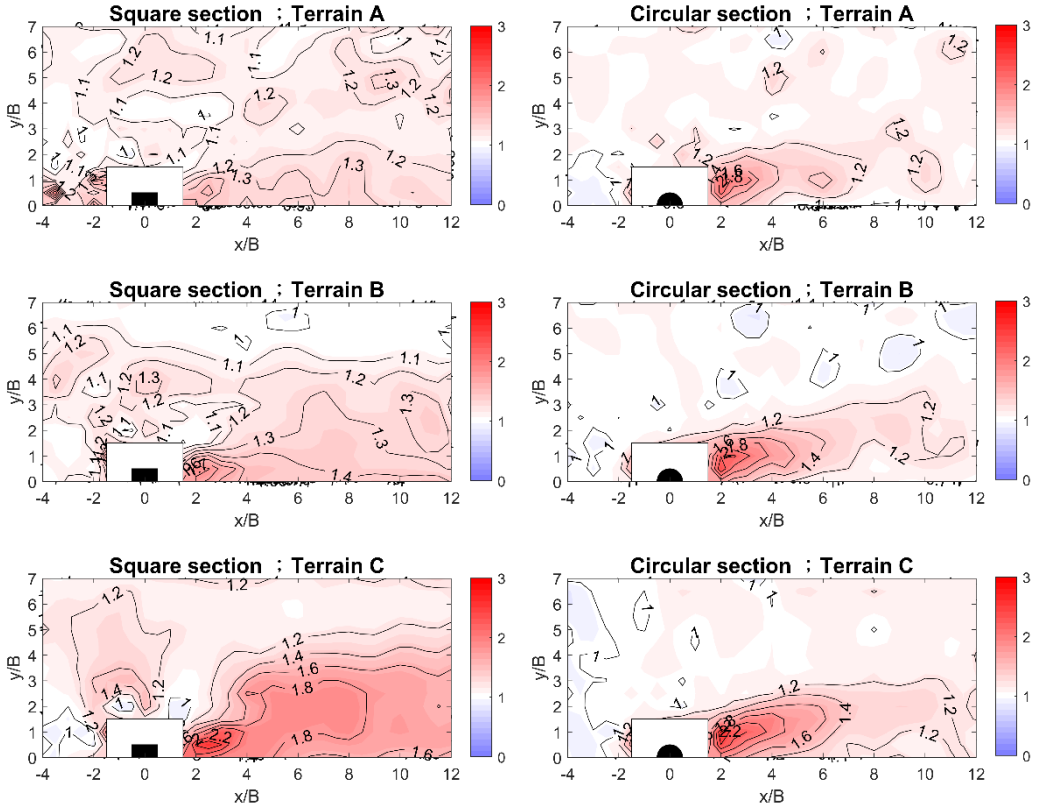

(a) Along-wind $EAIF_x$

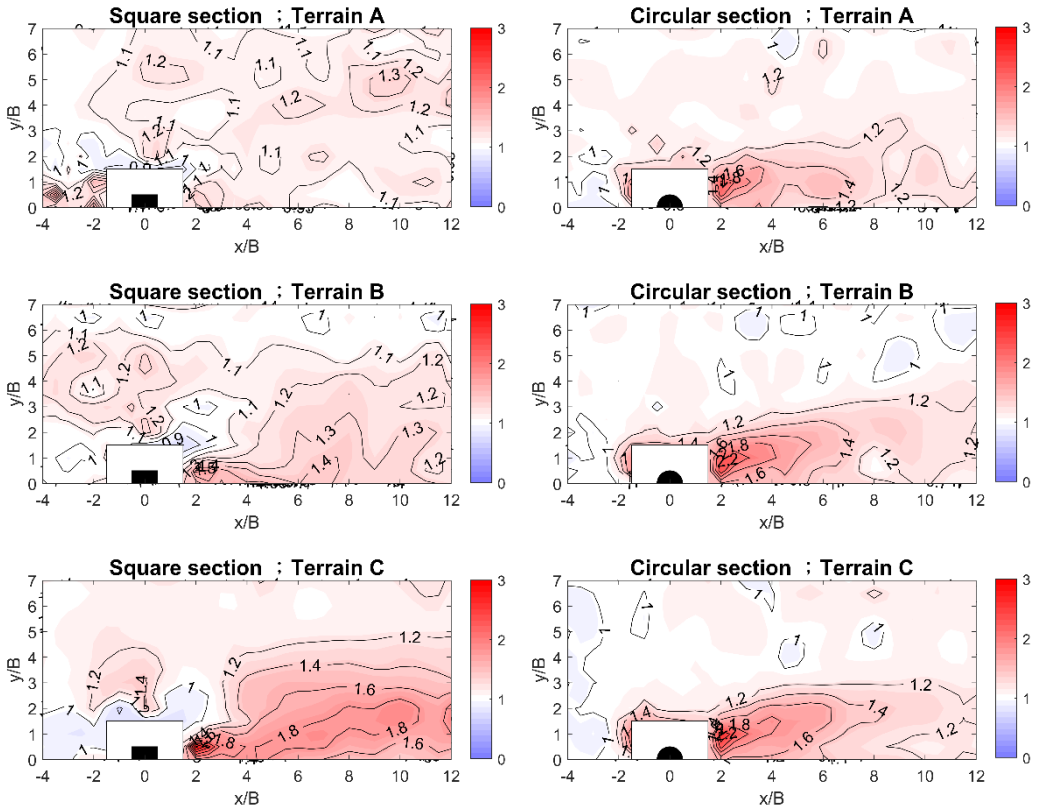

(b) Across-wind $EAIF_y$

Figure 9: Contours of acceleration interference factors: (a) Along-wind $EAIF_x$; (b) Across-wind $EAIF_y$.

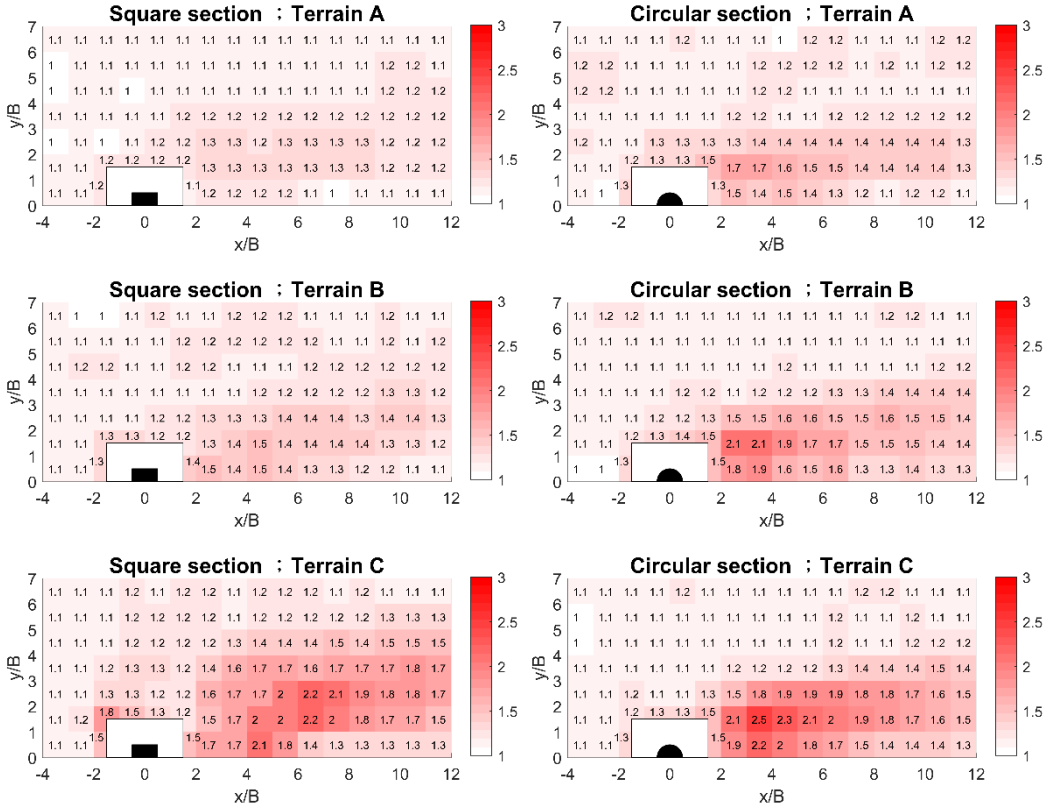

(a) Along-wind $EDIF_{x,des}$

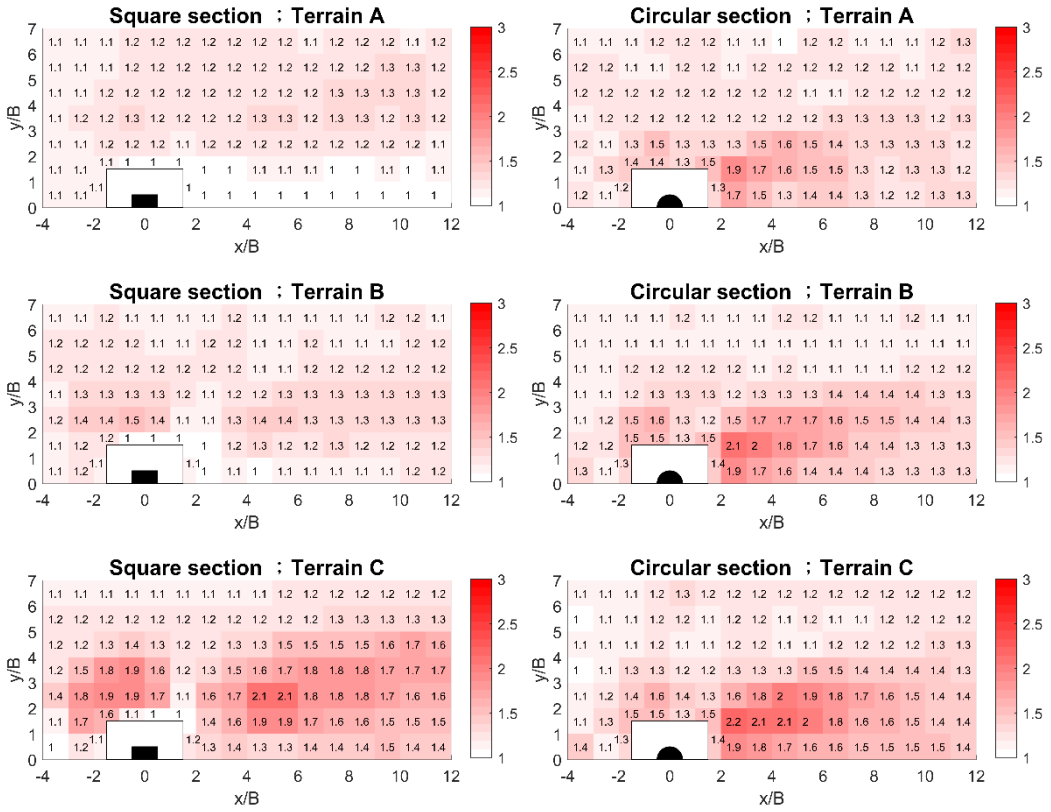

(b) Across-wind $EDIF_{y,des}$

Figure 10: Design interference factor maps for displacement response estimation: (a) Along-wind $EDIF_{x,des}$; (b) Across-wind $EDIF_{y,des}$.

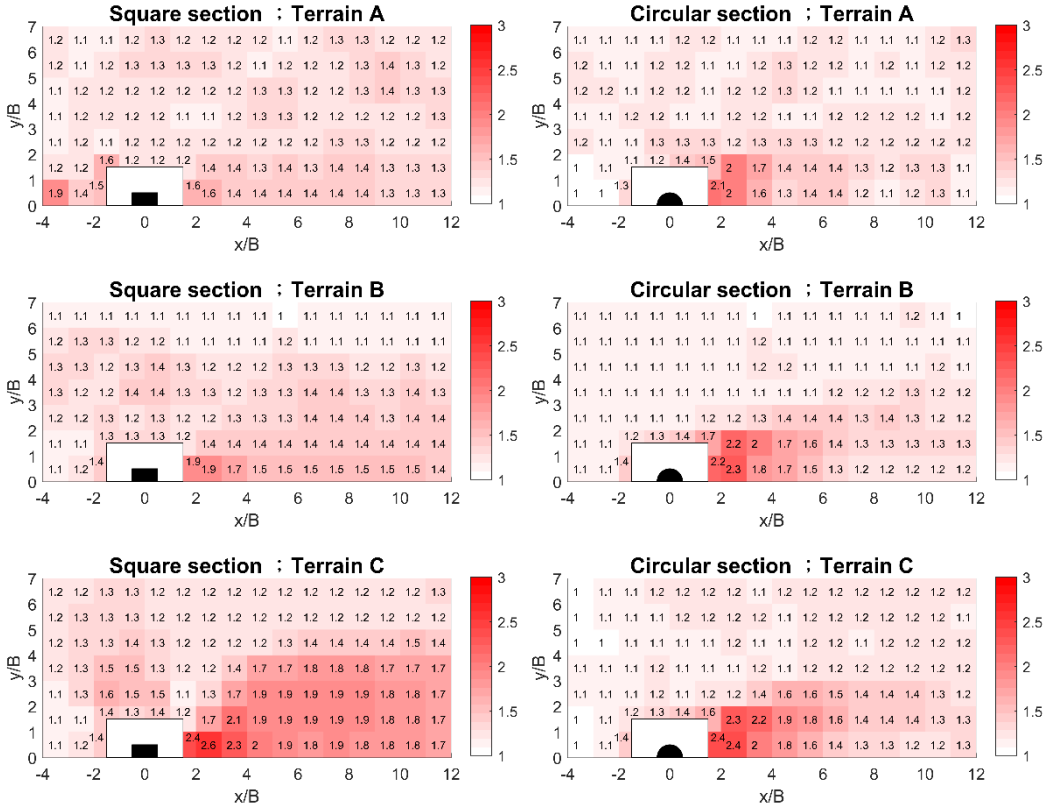

(a) Along-wind $EAIF_{x,des}$

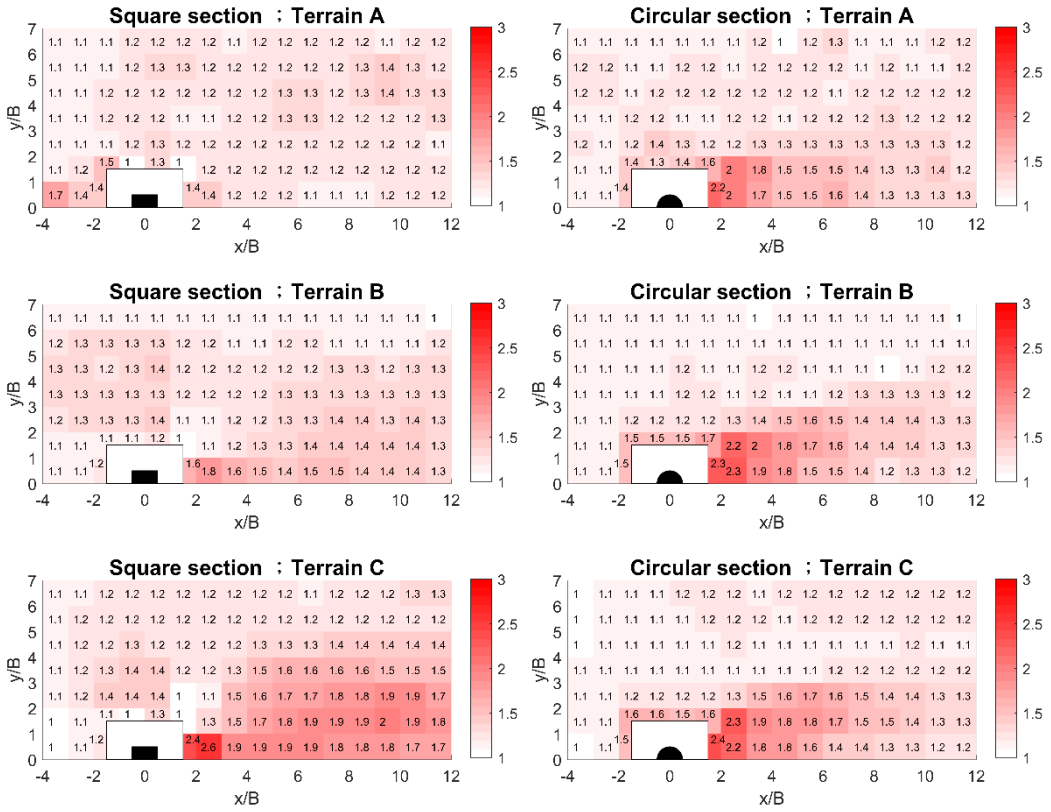

(b) Across-wind $EAIF_{y,des}$

Figure 11: Design interference factor maps for acceleration response estimation: (a) Along-wind $EAIF_{x,des}$; (b) Across-wind $EAIF_{y,des}$.

4. Conclusions

This study discussed the aerodynamic forces and wind-induced responses due to three common disturbance factors to the interference effects, including the terrain exposure effects, the interference location effects, and the shape effects of the principal and interfering buildings. Aerodynamic and response interference factors were defined and plotted in color contours to explain the interference mechanisms. Several observations were concluded as followings.

A belt-like region in the upwind area of the principal building is generally identified for the interference-induced reduction in the along-wind mean wind forces. The contour plots with the circular cross-sectional building show a narrower belt than the square one.

Terrain effects are indicated in the contour plots for fluctuating wind forces. The open country terrain (Terrain C) shows the most identifiable results among the three terrain exposures. Meanwhile, the shape effects show two different interference mechanisms near the two buildings. When the interfering building locates in the area surrounding the square principal building, a significant reduction in fluctuating across-wind force is found. In contrast, almost no reduction effect is observed near the circular one.

Amplification in the along-wind displacement response is generally distributed regardless of terrain and shape effects. The interference location of the most significant amplification is consistent with the references' commonly mentioned upstream area. The most amplification can be up to double the fluctuating response when the principal building is isolated. Similar results are observed for the along-wind acceleration responses.

Both amplification and reduction are similarly seen in the across-wind fluctuating displacement and acceleration responses. An interesting amplification in fluctuating displacement is observed at the side/downwind location for the square building, which is consistent with the downstream resonant phenomenon mentioned in Bailey and Kwok [3].

Finally, this study proposed several statistical steps to process the discretized maps of response interference factors. From the comparisons with other works (Mara *et al.* [33]), interference factors from wind tunnel tests in different facilities may have the same tendency but are often different in values. For practical designs, interference effects should be statistically quantified before being integrated into the codes or standards.

References

[1] J.W. Saunders, W.H. Melbourne, Buffeting effects of upstream buildings, Proceedings of the Fifth International Conference on Wind Engineering, Fort Collins, Colorado, USA, 1979.

[2] D. Surry, W. Mallais, Adverse local wind loads induced by adjacent building, Journal of Structural Engineering 109(3) (1983) 816-820. https://doi.org/10.1061/(ASCE)0733-9445(1983)109:3(816)

[3] P. A. Bailey, K. C. S. Kwok, Interference excitation of twin tall buildings, Journal of Wind Engineering and Industrial Aerodynamics 21(3) (1985) 323-338. https://doi.org/10.1016/0167-6105(85)90043-1

[4] J. Blessmann, J. D. Riera, Wind excitation of neighboring tall buildings, Journal of Wind Engineering and Industrial Aerodynamics 18(1) (1985) 91-103. https://doi.org/10.1016/0167-6105(85)90076-5

[5] A. Kareem, The effect of aerodynamic interference on the dynamic response of prismatic structures, Journal of Wind Engineering and Industrial Aerodynamics 25(3) (1987) 365-372. https://doi.org/10.1016/0167-6105(87)90028-6

[6] Y. Taniike, H. Inaoka, Aeroelastic behavior of tall buildings in wakes, Journal of Wind Engineering and Industrial Aerodynamics 28(1-3) (1988) 317-327. https://doi.org/10.1016/0167-6105(88)90128-6

[7] H. Sakamoto, H. Haniu, Aerodynamic forces acting on two square prisms placed vertically in a turbulent boundary layer, Journal of Wind Engineering and Industrial Aerodynamics 31(1) (1988) 41-66. https://doi.org/10.1016/0167-6105(88)90187-0

[8] Y. Taniike, Turbulence effect on mutual interference of tall buildings, Journal of Engineering Mechanics 117(3) (1991) 443-456. https://doi.org/10.1061/(ASCE)0733-9399(1991)117:3(443)

[9] Y. Taniike, Interference mechanism for enhanced wind forces on neighboring tall buildings, Journal of Wind Engineering and Industrial Aerodynamics 42(1-3) (1992) 1073-1083. https://doi.org/10.1016/0167-6105(92)90114-P

[10] M. Yahyai, K. Kumar, P. Krisha, P.K. Pande, Aerodynamic interference in tall rectangular buildings, Journal of Wind Engineering and Industrial Aerodynamics 41(1-3) (1992) 859-866. https://doi.org/10.1016/0167-6105(92)90506-6

[11] W.J. Zhang, K.C.S. Kwok, Y.L. Xu, Aeroelastic torsional behavior of tall buildings in wakes, Journal of Wind Engineering and Industrial Aerodynamics 51(2) (1994) 229-248. https://doi.org/10.1016/0167-6105(94)90006-X

[12] W.J. Zhang, Y.L. Xu, K.C.S. Kwok, Interference effects on aeroelastic torsional response of structurally asymmetric tall buildings, Journal of Wind Engineering and Industrial Aerodynamics 57(1) (1995) 41-61. https://doi.org/doi:10.1016/0167-6105(94)00098-X

[13] T.F. Sun, Z.F. Gu, Interference between wind loading on group of structures, Journal of Wind Engineering and Industrial Aerodynamics 54-55 (1995) 213-225. https://doi.org/10.1016/0167-6105(94)00051-E

[14] A.C. Khanduri, T. Stathopoulos, C. Bedard, Wind-induced interference effects on buildings – a review of the state-of-the-art." Engineering Structures, 20(7) (1998), 617-630. https://doi.org/10.1016/S0141-0296(97)00066-7

[15] A.C. Khanduri, T. Stathopoulos, C. Bedard, Generalization of wind-Induced interference effects for two buildings, Wind and Structures 3(4) (2000) 255-266. https://doi.org/10.12989/was.2000.3.4.255

[16] S.C. Luo, L.L. Li, D.A. Shah, Aerodynamic stability of the downstream of two tandem square-section cylinders, Journal of Wind Engineering and Industrial Aerodynamics 79(1-2) (1999) 79-103. https://doi.org/10.1016/S0167-6105(98)00111-1

[17] S. Thepmongkorn, G.S. Wood, K.C.S. Kwok, Interference effects on wind-induced coupled motion of a tall building, Journal of Wind Engineering and Industrial Aerodynamics 90(12-15) (2002) 1807-1815. https://doi.org/10.1016/S0167-6105(02)00289-1

[18] U.F. Tang, K.C.S. Kwok, Interference excitation mechanisms on a 3DOF aeroelastic CAARC building model, Journal of Wind Engineering and Industrial Aerodynamics 92(14-15) (2004) 1299-1314. https://doi.org/10.1016/j.jweia.2004.08.004

[19] Z.N. Xie, M. Gu, Mean interference effects among tall buildings, Engineering Structures 26(9) (2004) 1173-1183. https://doi.org/10.1016/j.engstruct.2004.03.007

[20] Z.N. Xie, M. Gu, Simplified formulas for evaluation of wind-induced interference effects among three tall buildings, Journal of Wind Engineering and Industrial Aerodynamics 95(1) (2007) 31-52. https://doi.org/10.1016/j.jweia.2006.05.003

[21] P. Huang, M. Gu, Experimental study on wind-induced dynamic interference effects between two tall buildings, Wind and Structures 8(3) (2005) 147-161. https://doi.org/10.12989/was.2005.8.3.147

[22] C.M. Cheng, Y.Y. Lin, J. Wang, J.C. Wu, C.H. Chang, The aerodynamic database for the interference effects of adjacent tall buildings, Proceedings of the 12th International Conference on Wind Engineering (ICWE12), Cairns, Australia, 2007.

[23] J.G. Zhao, K.M. Lam, Interference effect in a group of tall buildings closely arranged in an L- or T-Shaped pattern, Wind and Structures 11(1) (2008) 1-18. https://doi.org/10.12989/was.2008.11.1.001

[24] K.M. Lam, M.Y.H. Leung, J.G. Zhao, Interference effects on wind loading of a row of closely spaced tall buildings, Journal of Wind Engineering and Industrial Aerodynamics 96(5) (2008) 562-583. https://doi.org/10.1016/j.jweia.2008.01.010

[25] K.M. Lam, J.G. Zhao, M.Y.H. Leung, M. Y. H., Wind-induced loading and dynamic responses of a row of tall buildings under strong interference, Journal of Wind Engineering and Industrial Aerodynamics 99 (2011) 573-583. https://doi.org/10.1016/j.jweia.2011.02.006

[26] Y. Hui, Y. Tamura, A. Yoshida, Mutual interference effects between two high-rise building models with different shapes on local peak pressure coefficients, Journal of Wind Engineering and Industrial Aerodynamics 104-106 (2012) 98-108. https://doi.org/10.1016/j.jweia.2012.04.004

[27] Y. Hui, Y. Tamura, A. Yoshida, H. Kikuchi, Pressure and flow field investigation of interference effects on external pressures between high-rise buildings, Journal of Wind Engineering and Industrial Aerodynamics 115 (2013) 150-161. https://doi.org/10.1016/j.jweia.2013.01.012

[28] Y. Hui, A. Yoshida, Y. Tamura, Y., Interference effects between two rectangular-section high-rise buildings on local peak pressure coefficients, Fluids and Structure 37 (2013) 120-133. https://doi.org/10.1016/j.jfluidstructs.2012.11.007

[29] F.M. Fang, C.Y. Chung, Y.C. Li, W.C. Liu, P.K. Lei, The acrosswind response of the downwind prism in a twin-prism system with a staggered arrangement, Wind and Structures 17(3) (2013) 245-262. https://doi.org/10.12989/was.2013.17.3.245

[30] W.S. Kim, Y. Tamura, A. Yoshida, Interference effects on local peak pressures between two buildings, Journal of Wind Engineering and Industrial Aerodynamics 99(5) (2011) 584-600. https://doi.org/10.1016/j.jweia.2011.02.007

[31] W.S. Kim, Y. Tamura, A. Yoshida, Simultaneous measurement of wind pressures and flow patterns for buildings with interference effect, Advances in Structural Engineering 16(2) (2013) 287-305. https://doi.org/10.1260/1369-4332.16.2.287

[32] W.S. Kim, Y. Tamura, A. Yoshida, Interference effects on aerodynamic wind forces between two buildings, Journal of Wind Engineering and Industrial Aerodynamics 147 (2015) 186-201. https://doi.org/10.1016/j.jweia.2015.10.009

[33] T.G. Mara, B.K. Terry, T.C.E. Ho, N. Isyumov, Aerodynamic and peak response interference factors for an upstream square building of identical height, Journal of Wind Engineering and Industrial Aerodynamics 133 (2014) 200-210. https://doi.org/10.1016/j.jweia.2014.06.010

[34] X.F. Yu, Z.N. Xie, J.B. Zhu, M. Gu, Interference effects on wind pressure distribution between two high-rise buildings, Journal of Wind Engineering and Industrial Aerodynamics 142 (2015) 188-197. https://doi.org/10.1016/j.jweia.2015.04.008

[35] Y.L. Lo, Y.C. Kim, Y.C. Li, Downstream interference effect of high-rise buildings under turbulent boundary layer flow, Journal of Wind Engineering and Industrial Aerodynamics 159 (2016) 19-35. https://doi.org/10.1016/j.jweia.2016.10.002

[36] Y.L. Lo, Y.C. Kim, A. Yoshida, Effects of aerodynamic modification mechanisms on interference from neighboring buildings, Journal of Wind Engineering and Industrial Aerodynamics 168 (2017) 271-287. https://doi.org/10.1016/j.jweia.2017.06.018

[37] X.F. Yu, Z.N. Xie, M. Gu, Interference effects between two tall buildings with different section sizes on wind-induced acceleration, Journal of Wind Engineering and Industrial Aerodynamics 182 (2018) 16-26. https://doi.org/10.1016/j.jweia.2018.09.012

[38] Y.L. Lo, Y.C. Li, Y.C. Kim, Downstream interference effect of low-Scruton-number high-rise buildings under turbulent boundary layer flow, Journal of Wind Engineering and Industrial Aerodynamics 198 (2020). https://doi.org/10.1016/j.jweia.2020.104101

[39] A.G. Davenport, Gust loading factors, Journal of the Structural Division ASCE-SECI 93(3) (1967). https://doi.org/10.1061/JSDEAG.0001692

[40] GB 50009-2012 Load code for the design of building structures, China Architecture Publishing and Media Co., Ltd., Beijing, China, 2012.

[41] Recommendations for Loads on Buildings (2015), Architectural Institute of Japan (AIJ), Tokyo, Japan, 2015.

[42] ISO 10137:2007 Bases for design of structures - Serviceability of buildings and walkways against vibrations, International Standard Organization, Geneva Switzerland, 2018.

[43] AWES-QAM-1-2019 Quality assurance manual: Wind engineering studies of buildings, Australasian Wind Engineering Society (AWES), Australia, 2019.

[44] C.M. Cheng, C.L. Fu, Characteristic of wind loads on a hemispherical dome in smooth flow and turbulent boundary layer flow, Journal of Wind Engineering and Industrial Aerodynamics 98(6-7) (2010) 328-344. https://doi.org/10.1016/j.jweia.2009.12.002

[45] J.D. Holmes, S.A. Bekele, Wind Loading of Structures. 4th ed, CRC Press, New York, United States, 2021.

[46] Taiwan Wind Code for Buildings 2015, Construction and Planning Agency, Ministry of Interior, R.O.C., Taipei, Taiwan, 2015.

[47] Y. Tamura, Amplitude dependency of damping in building and estimation techniques, Proceedings of the 12th Australasian Wind Engineering Society Workshop, Queenstown, New Zealand, 2006.

[48] Y. Tamura, Amplitude dependency of damping in building and critical tip drift Ratio, International Journal of High-Rise Building 1(1) (2012) 1-13. https://doi.org/10.21022/IJHRB.2012.1.1.001

[49] Y.L. Lo, Y.C. Kim, Estimation of wind-induced response on high-rise buildings immersed in interfered flow, Journal. of Applied Science and Engineering 22(3) (2019) 429-448. https://doi.org/10.6180/jase.201909_22(3).0005